

# Non-Linear Numerical Simulations of Magneto-Acoustic Wave Propagation in Small-Scale Flux Tubes

E. Khomenko<sup>1,2</sup> · M. Collados<sup>1</sup> · T. Felipe<sup>1</sup>

© Springer ●●●

**Abstract** We present results of non-linear, 2D, numerical simulations of magneto-acoustic wave propagation in the photosphere and chromosphere of small-scale flux tubes with internal structure. Waves with realistic periods of three to five minutes are studied, after applying horizontal and vertical oscillatory perturbations to the equilibrium model. Spurious reflections of shock waves from the upper boundary are minimized thanks to a special boundary condition. This has allowed us to increase the duration of the simulations and to make it long enough to perform a statistical analysis of oscillations. The simulations show that deep horizontal motions of the flux tube generate a slow (magnetic) mode and a surface mode. These modes are efficiently transformed into a slow (acoustic) mode in the  $v_A < c_S$  atmosphere. The slow (acoustic) mode propagates vertically along the field lines, forms shocks and remains always within the flux tube. It might deposit effectively the energy of the driver into the chromosphere. When the driver oscillates with a high frequency, above the cut-off, non-linear wave propagation occurs with the same dominant driver period at all heights. At low frequencies, below the cut-off, the dominant period of oscillations changes with height from that of the driver in the photosphere to its first harmonic (half period) in the chromosphere. Depending on the period and on the type of the driver, different shock patterns are observed.

**Keywords:** Photosphere, Chromosphere, Magnetohydrodynamics, Oscillations, Magnetic fields

## 1. Introduction

Solar magnetic structures show a continuous distribution of fluxes and sizes. In active regions, the field strength concentrated in large-scale structures (sunspots and pores) can be as large as 2 – 4 kG. In plage and network areas, the average flux decreases to several hundreds Gauss. However, individual flux tubes in these areas can have intrinsic magnetic field strength similar to that of solar pores, *i.e.* 1 – 2 kG. The

---

<sup>1</sup> Instituto de Astrofísica de Canarias, 38205, C/ Vía Láctea, s/n, Tenerife, Spain; email: khomenko@iac.es, mcv@iac.es, tobias@iac.es

<sup>2</sup> Main Astronomical Observatory, NAS, 03680 Kyiv, Zabolotno str. 27, Ukraine

decrease of the average flux is caused mainly by the decrease of the size of the magnetic features, *i.e.* their filling factor.

The observed photospheric brightness of the magnetic structures is in close relationship with their flux and size (see for example Berger, Rouppe van der Voort, and Löfdahl, 2007). Large-scale features like sunspots and pores appear dark in photospheric observations. Plage and facular flux tubes appear as bright features (see for example Figure 7 in Berger, Rouppe van der Voort, and Löfdahl, 2007).

Due to their larger size, sunspots show horizontal gradients of the magnetic field strength and inclination. Instead, small-scale flux tubes possess a more homogeneous field with a rather sharp transition between the magnetized and non-magnetized surroundings. From the point of view of wave propagation, it is important to realize that the temperature at a given geometrical height is different in the different structures. Temperature and magnetic field define the characteristic wave propagation speeds, *i.e.* sound speed,  $c_S$ , and Alfvén speed,  $v_A$ , as well as the acoustic cut-off frequency,  $\omega_C$ , and the height of the transformation layer where  $c_S$  is equal to  $v_A$  and different wave modes can interact. These parameters can be rather different in large-scale dark structures and small-scale bright structures. Thus, it is not surprising that the observed properties of waves in sunspots, network, and plage areas are rather different.

### 1.1. Sunspots and Pores

Several decades of studies of sunspot oscillations can be summarized as follows. Waves observed at different layers of the atmosphere of sunspots umbrae and penumbrae seem to be the manifestation of the same phenomenon (see *e.g.* Maltby *et al.*, 1999, 2001, Brynildsen *et al.*, 2000, 2002, Christopoulou, Georgakilas, and Koutchmy, 2000, 2001, Rouppe van der Voort *et al.*, 2003, Tziotziou *et al.*, 2006). In the photosphere, five-minute oscillations are observed in sunspot umbrae and penumbrae and in solar pores (Bogdan and Judge, 2006). Wave propagation is linear with amplitudes of several hundreds of  $\text{m s}^{-1}$  and is parallel to the magnetic field lines (see *e.g.* Gurman and Leibacher, 1984, Lites, 1984, Collados *et al.*, 2001, Centeno, Collados, and Trujillo Bueno, 2006, Bloomfield, Lagg, and Solanki, 2007). Magnetic field oscillations of a few Gauss are detected in the deeper layers and attempts have been made to interpret these oscillations in terms of fast and slow MHD waves (*e.g.* Rüedi *et al.*, 1998, Lites *et al.*, 1998, Bellot Rubio *et al.*, 2000, Khomenko, Collados, and Bellot Rubio, 2003).

In the chromosphere, the dominant period of oscillations decreases and shock waves are observed with a three-minute periodicity in sunspot umbrae and in pores (Lites, 1984, 1986, 1988, Socas-Navarro, Trujillo Bueno, and Ruiz Cobo, 2000, Centeno, Collados, and Trujillo Bueno, 2006, Tziotziou *et al.*, 2007). The amplitudes of the observed shocks are in the range of  $5 - 15 \text{ km s}^{-1}$ , depending on the size of the structure. In pores, shocks are weaker (Centeno, Collados, and Trujillo Bueno, 2006). Umbral flashes also show a three-minute periodicity. In contrast, in the penumbra, the shock behavior of waves with five-minute periodicity is detected for running penumbral waves even at chromospheric heights (Tziotziou *et al.*, 2006). Waves observed in the transition region and the corona conserve these properties (De Moortel *et al.*, 2002, Marsh and Walsh, 2005, 2006, Maltby *et al.*, 1999, 2001, Brynildsen *et al.*, 2000, 2002, Christopoulou, Georgakilas, and Koutchmy, 2000, 2001). Wave propagation from the photospheric pulse into the chromosphere and higher layers is along the magnetic field lines for both three and five minutes perturbations.

## 1.2. Plages, Facular regions, and Network

Bright magnetic field structures like plages, facular regions, and network manifest five-minute linear oscillations in the photosphere and the oscillations maintain the five minute periodicity in the chromosphere and larger heights (Lites, Rutten, and Kalkofen, 1993, Krijger *et al.*, 2001, De Pontieu, Erdelyi, and de Wijn, 2003, Centeno, Collados, and Trujillo Bueno, 2006, Bloomfield *et al.*, 2006, Vecchio *et al.*, 2007). Shock occurrence is much lower in these quiet Sun regions with enhanced flux (Krijger *et al.*, 2001, Centeno, Collados, and Trujillo Bueno, 2006). The velocity oscillation amplitudes in the chromosphere do not reach values as large as in sunspots and stay within  $2-4 \text{ km s}^{-1}$ . Waves at photospheric and chromospheric layers seem to be correlated and vertical propagation along the vertical magnetic fields seem to dominate (Krijger *et al.*, 2001, Centeno, Collados, and Trujillo Bueno, 2006, Vecchio *et al.*, 2007). Curiously, there are areas with enhanced three-minute power surrounding the strong magnetic field concentrations, possibly related to flux tube canopies (aureoles, see Braun and Lindsey, 1999, Thomas and Stanchfield, 2000, Krijger *et al.*, 2001, Judge, Tarbell, and Wilhelm, 2001). In the higher coronal layers, loops connecting sunspots oscillate with three minutes and the loops connecting network and plage regions oscillate with five minute periods (De Moortel *et al.*, 2002).

Thus, the wave properties are distinctly different in large-scale and small-scale magnetic features. The difference in oscillation properties is present through the whole solar atmosphere and should be a consequence of the thermal and magnetic properties of these structures.

## 1.3. Theoretical Models

A number of theoretical mechanisms have been proposed to explain the oscillation spectra at different heights in magnetic structures and to interpret the observed oscillations in terms of MHD waves. Zhugzhda and Locans (1981), Gurman and Leibacher (1984), and Zhugzhda (2007) argue that the observed spectrum of sunspot umbral oscillations in the chromosphere is due to the temperature gradients of the atmosphere acting as an interference filter for linear three-minute period acoustic waves. On the other hand, it has been demonstrated by Fleck and Schmitz (1991) that the change of the period with height from five to the three minutes is a basic phenomena occurring even in an isothermal atmosphere for linear waves due to the resonant excitation at the atmospheric cut-off frequency. In the case of the solar atmosphere, the temperature minimum gives rise to the three-minute cut-off period. Later, the same authors found that, due to non-linear shock interaction and overtaking, the frequency of acoustic oscillations also changes with height (Fleck and Schmitz, 1993). The response of the solar atmosphere to an adiabatic shock wave leads to a natural appearance of the three-minute peak in the oscillation power spectra, in the case the underlying photosphere has a five-minute periodicity. A third mechanism was shown to explain the three-minute periodicity of calcium bright grains in the quiet Sun: with a spectrum of periods in the photosphere with a peak at five minutes, this distribution changes to one with a maximum at the acoustic cut-off because at longer periods the energy falls off exponentially with height (Carlsson and Stein, 1997). These mechanisms may explain the shift with height of the period of oscillations from five to three minutes observed in sunspots.

The question remains: why is there not such a shift in small-scale structures of plages and network regions? De Pontieu, Erdelyi, and Stewart (2004) argue that the inclination of the magnetic field may play an important role. If (acoustic or slow MHD) waves have a preferred direction of propagation defined by the magnetic field, the effective cut-off frequency is lowered by the cosine of the inclination angle with respect to the vertical. This allows evanescent waves to propagate. It should be recalled, however, that mainly vertical propagation is observed in the photosphere and chromosphere in plage regions (see *e.g.* Krijger *et al.*, 2001, Centeno, Collados, and Trujillo Bueno, 2006), thus it is unclear whether the mechanism suggested by De Pontieu, Erdelyi, and Stewart (2004) is at work. Alternatively, the decrease of the effective acoustic cut-off frequency can be produced by taking into account the radiative losses of acoustic oscillations (Roberts, 1983; Centeno, Collados, and Trujillo Bueno, 2006). If the radiative relaxation time is effectively small (as expected in small-scale magnetic structures, transparent to radiation), the cut-off frequency can be reduced and evanescent waves can propagate.

All works cited above apply the theory of acoustic waves in idealized atmospheres in order to explain the observed oscillation properties in magnetic structures. In magnetized atmospheres, different wave types can exist and different modes can be observed depending on the magnetic field configuration and the height of the transformation layer ( $c_S = v_A$ ) relative to the height of the formation of the spectral lines used in observations. Bogdan *et al.* (2003), Rosenthal *et al.* (2002), Hasan and Ulmschneider (2004), Hasan *et al.* (2003, 2005), addressed this question in their simulations of magneto-acoustic waves in non-trivial magnetic configurations. They pointed out the importance of defining the mode type and the mode conversion height when interpreting the observations. Due to mode mixing at the transformation layer, no correlation may be observed between perturbations below and above the  $c_S = v_A$  height.

All these arguments point of towards the need to have realistic, self-consistent, and systematic models of the wave spectrum in magnetic structures. It is necessary to include non-trivial magnetic field configurations in order to allow the existence of different mode types and mode conversion. Non-linearities should be taken into account for waves propagating into the chromosphere. The thermal structure should be realistic in order to make possible the reflection of waves with frequencies below the cut-off. Radiative damping also plays an important role, in particular to estimate the amount of energy that may be deposited in the higher atmosphere due to waves. In the present work we address several of the above questions. We perform non-linear numerical modeling of magneto-acoustic waves in small-scale magnetic flux tubes with internal structure. We consider waves with realistic periods of three and five minutes, which has never been done before for non-trivial magnetic configurations. We study the mode transformation and oscillation spectra at different heights from 0 to 2000 km as a function of the type of the driver and its period. At present, radiative damping of oscillations is not taken into account. This question will be addressed in a separate paper.

## 2. Numerical Model

We solve the basic equations of the ideal MHD, written in conservative form:

$$\frac{\partial \rho}{\partial t} + \vec{\nabla} \cdot (\rho \vec{V}) = 0, \quad (1)$$

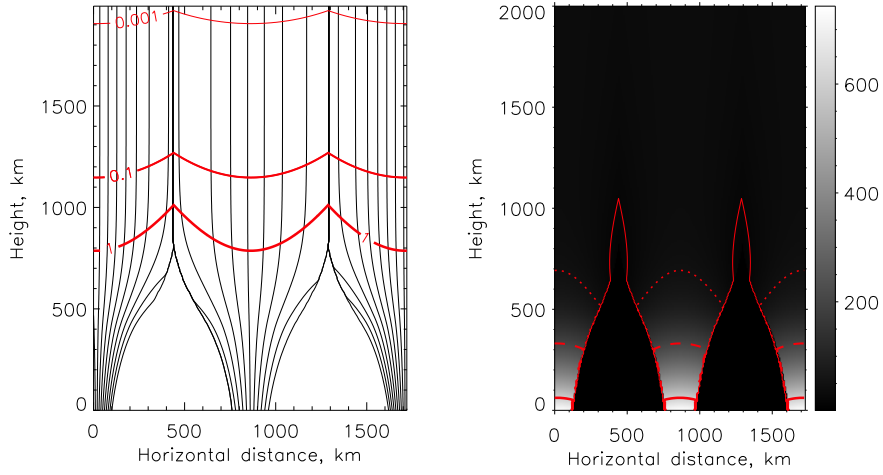


**Figure 1.** Second-order flux tube magnetostatic model, calculated after Pneuman, Solanki, and Stenflo (1986). The tube radius is equal to 100 km in the photosphere. Left panel: magnetic field lines and contours of plasma  $\beta$  (defined as  $c_s^2/v_A^2$ ), with values indicated on each contour. Right panel: distribution of the magnetic field strength.

$$\frac{\partial(\rho\vec{V})}{\partial t} + \vec{\nabla} \cdot [\rho\vec{V}\vec{V} + (P + \frac{\vec{B}^2}{8\pi})\mathbf{I} - \frac{\vec{B}\vec{B}}{4\pi}] = \rho\vec{g}, \quad (2)$$

$$\frac{\partial E}{\partial t} + \vec{\nabla} \cdot [(E + P + \frac{\vec{B}^2}{8\pi})\vec{V} - \vec{B}(\frac{\vec{B} \cdot \vec{V}}{4\pi})] = \rho\vec{V} \cdot \vec{g} + \rho Q, \quad (3)$$

$$\frac{\partial \vec{B}}{\partial t} = \vec{\nabla} \times (\vec{V} \times \vec{B}), \quad (4)$$

where  $\mathbf{I}$  is the diagonal identity tensor and  $E$  is the total energy:

$$E = \frac{1}{2}\rho V^2 + \frac{P}{\gamma - 1} + \frac{B^2}{8\pi}. \quad (5)$$

All other symbols have their usual meaning. The numerical code solving these equations was used previously in Khomenko and Collados (2006) and is described in details in that paper. For the present work, the code has been improved to solve the fully non-linear equations. One of the main differences between our code and any other standard MHD code is that we solve equations for perturbations (including all non-linear terms), the magnetostatic equilibrium being analytically subtracted from the above system of equations.

The term describing energy losses, ( $Q$ ), is set to zero in the present study. A Perfect Matching Layer (PML) boundary condition (Berenger, 1994) is applied to the sides and top boundaries of the simulation domain. It is found to perform rather well in our simulations. Tests have shown that wave reflection from the upper boundary can be reduced to a few percent even for shock waves with Mach number of two or three. This has allowed us to perform longer temporal series of simulations, not stopping them at the time when the fastest wave reaches the upper boundary,

**Table 1.** Characteristic parameters of the model flux tube taken at the flux tube axis.

Parameter	$z=0$ km	$z=2000$ km
Temperature (K)	6420	7175
Magnetic field (G)	743	37
Sound speed ( $\text{km s}^{-1}$ )	8	10
Alfven speed ( $\text{km s}^{-1}$ )	4	394
$c_S^2/v_A^2$	4	$7 \times 10^{-4}$
Pressure scale height (km)	151	228
Cut-off period (s)	230	280

and to analyze these simulations in a statistical way, similar to observations. The boundary conditions and other numerical details are described elsewhere (Khomenko and Collados, 2006). The simulations analyzed below are done in two dimensions.

At the bottom (photospheric) boundary, we specify either a vertical or horizontal velocity as a function of time and horizontal coordinate ( $x$ ):

$$V_{x,z}(x, t) = V_0 \sin(\omega t) \times \exp(-(x - x_0)^2 / 2\sigma^2). \quad (6)$$

The perturbation is localized in the  $x$ -axis and has a Gaussian shape in this direction. The horizontal size of the pulse  $\sigma = 160$  km, initial amplitude at the photosphere  $V_0 = 200 \text{ m s}^{-1}$  and  $x_0$  corresponds to the tube axis.

### 3. Magnetostatic Model

In order to construct an initial magnetostatic structure, we have followed the method described in Pneuman, Solanki, and Stenflo (1986). The equations for magnetostatic equilibrium have been written in cylindrical coordinates. All the variables were expanded in a power series in the horizontal radial coordinate  $r$ . The series have been truncated after the second order in  $r$ . After some manipulations with the equations, one single equation can be obtained for the vertical stratification of the magnetic field strength at the flux tube axis (for details, see Pneuman, Solanki, and Stenflo, 1986). This equation has been solved numerically using an iterative interpolation scheme from Korn and Korn (2000). Once the magnetic field at the axis is obtained, all of the other variables can be calculated from analytical expressions. The free parameters of the model are: magnetic field strength and flux tube radius at the base of photosphere and filling factor. The latter parameter allows us to produce a smooth merging of flux tubes at some chromospheric height. By varying these parameters, we have obtained a solution with desired properties concerning the height of the transformation layer  $c_S = v_A$ , inclination of field lines, and size of the tube. The temperatures inside and outside the flux tube were kept constant at all heights. The initial stratification of the thermodynamic parameters were taken from the VAL-C atmospheric model (Vernazza, Avrett, and Loeser, 1981). Table 1 and Figure 1 summarize the magnetic and thermal properties of our magnetostatic solution.

Since our model flux tube is a second-order approximation to a thin flux tube, it has horizontal variations of magnetic field strength, pressure, *etc.* This approximation

also gives rise to horizontal and vertical variations of the plasma  $\beta$  (note that through the present paper we define  $\beta$  as  $c_S^2/v_A^2$ ). The transition between the outside and inside atmospheres is rather sharp. Due to pressure balance, the gas pressure is smaller inside than outside the flux tube. The magnetic field lines fan out until a certain height, where nearby flux tubes merge together. After that height, the magnetic field becomes vertical and almost homogeneous in the horizontal direction.

The magnetostatic model shown in Figure 1 was perturbed by either a vertical or a horizontal driver, as follows from Equation (6). The results of the simulations for different driving periods are described in the remainder of the paper.

#### 4. “Mode Conversion” Nomenclature

There is a varying usage of the term “mode conversion” both in astrophysics and in plasma physics literature.

On the one side, the term “mode conversion” is used when the mode changes from slow to fast or the other way around (see, *e.g.* Cally (2006)). The transformation of a slow (magnetic) mode into slow (acoustic) mode is not called “mode conversion”, but instead “the changing of the character of slow mode” (same for the fast mode).

On the other side, in a later paper by Cally (2007), the terms “conversion” and “transmission” are used. The term “conversion” is used to describe the change from acoustic to magnetic nature of the wave or the other way around, *i.e.* slow–slow or fast–fast. The term “transmission” is used to describe the change from slow to fast or from fast to slow. This terminology used in parts of the plasma physics literature as well.

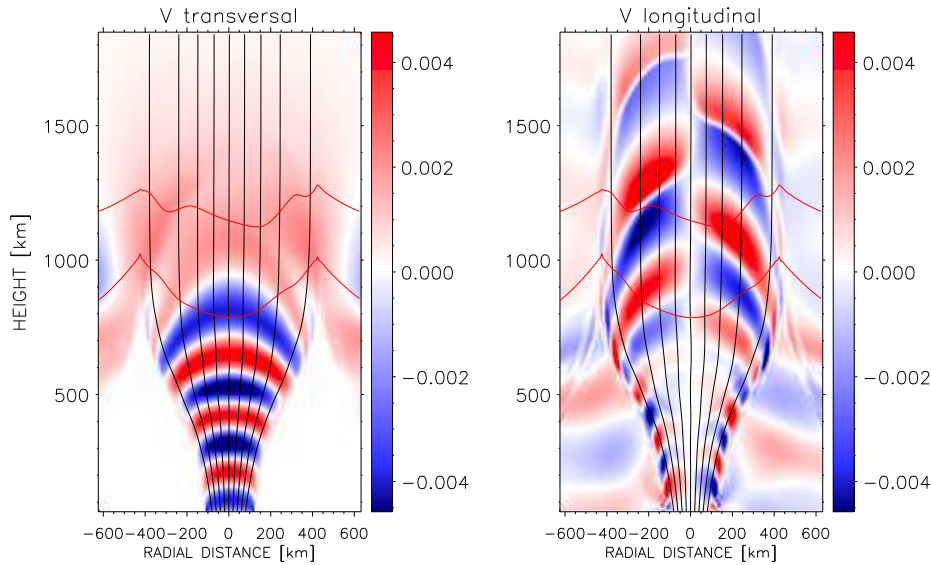
Since there seems to be no standard to describe what a mode conversion is, we find it necessary to define the nomenclature we utilize below in the paper. We use the term “mode conversion” in a more general sense. When the propagation speed of wave changes from fast to slow, we call it “mode conversion from fast mode to slow mode” (the same for the opposite). When the physics of the restoring force changes from magnetic to acoustic, we call it “mode conversion from slow (magnetic) mode to slow (acoustic) mode” (the same for the fast mode).

#### 5. Horizontal Driving at 50 Seconds

Simulations of short-period (*i.e.* short-wavelength) waves have the advantage that they make possible to understand easily what types of wave modes are generated and what transformations take place.

Figure 2 gives a snapshot of the transverse and longitudinal velocity components at an elapsed time of 340 seconds after the start of the simulations, and Figure 3 gives the temporal evolution of this simulation during the early stages. At each point, the transverse component is normalized to  $\sqrt{v_A \rho_0}$ , and the longitudinal component is normalized to  $\sqrt{c_S \rho_0}$ . This normalization allows us to compare the energy fluxes in both components for the case of the linear, short-wavelength perturbations.

The periodic horizontal driver located at the lower boundary in the high- $\beta$  regime generates primarily a slow magnetic mode, detected in the transverse velocity perturbation inside the flux tube at lower heights. Due to the Gaussian shape of the driver, the fast mode is also generated. It can be seen at the early snapshots in



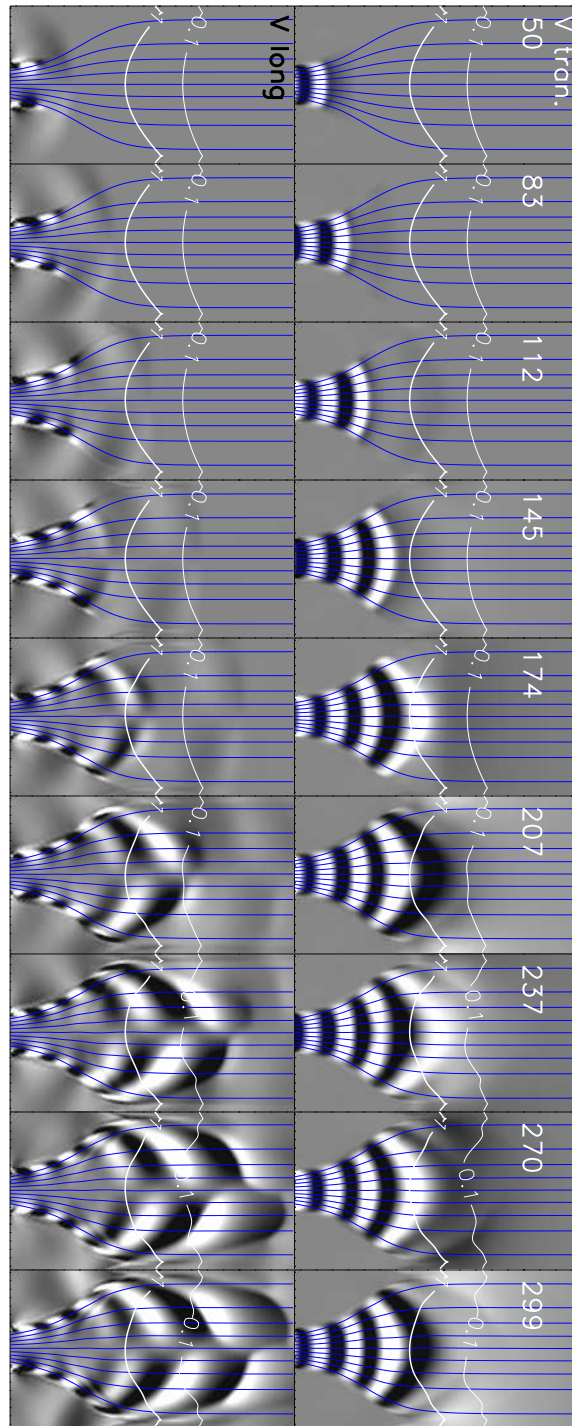
**Figure 2.** Snapshot of the simulations excited with a horizontal driver at 50 seconds. The panels show the transverse (perpendicular to the magnetic field) and longitudinal (parallel to the magnetic field) velocity components at an elapsed time of 340 seconds after the start of the simulations. The transverse component is normalized to  $\sqrt{v_A \rho_0}$  and the longitudinal component is normalized to  $\sqrt{c_S \rho_0}$  in order to highlight the variations of the energy flux as a function of height. The black lines represent the magnetic field lines. The two red lines are contours of constant  $c_S^2/v_A^2$ , the thick line corresponding to  $v_A = c_S$  and the thin line to  $c_S^2/v_A^2 = 0.1$ . Note the change of the position of both curves, compared to Figure 1, produced by wave motions.

Figure 3 (up to 240 seconds after the start of the simulation) as a weak perturbation in longitudinal velocity propagating rapidly up and having a longer wavelength. It can be seen that the fast wave is rather weak and does not play a major role at the stationary stage of the simulation. Its contribution to the total energy flux at the upper atmosphere is only minor. Note, also, that the fast wave is present outside the flux tube in the field-free atmosphere. This is due to the fact that the width of the driver ( $\sigma$ ) is larger than the radius of the flux tube [Equation(6)].

The slow mode generated at the bottom propagates vertically upward changing the curvature of the wave front due to the horizontal gradients in the Alfvén speed inside the flux tube. Note that there is no corresponding perturbation in the longitudinal velocity inside the tube. This confirms that the slow mode is purely transverse. In addition to this slow magnetic mode, horizontal motions at the lower boundary also generate a surface mode. It can be seen very well in the snapshot of the longitudinal velocity. This mode is localized on the magnetic–non-magnetic interfaces and follows the shape of the tube. The perturbation associated with the surface mode decays exponentially away from the tube boundary inwards and outwards. The surface mode is longitudinal and can be distinguished in the simulations until the height where flux tubes merge and the magnetic field and other parameters become homogeneous.

In the vicinity of the  $c_S = v_A$  layer, both the slow magnetic mode and the surface mode transfer most of their energy to the slow acoustic mode. This transformation





**Figure 3.** Time series of snapshots of the transverse (right) and longitudinal (left) velocities in the simulation with a horizontal driver at 50 seconds, showing the early stages of the evolution. Numbers give the elapsed time in seconds since the start of the simulation. The transverse component is normalized to  $\sqrt{v_A \rho_0}$  and the longitudinal component is normalized to  $\sqrt{c_S \rho_0}$ . Each snapshot includes 900 km in horizontal and 2000 km in vertical directions.

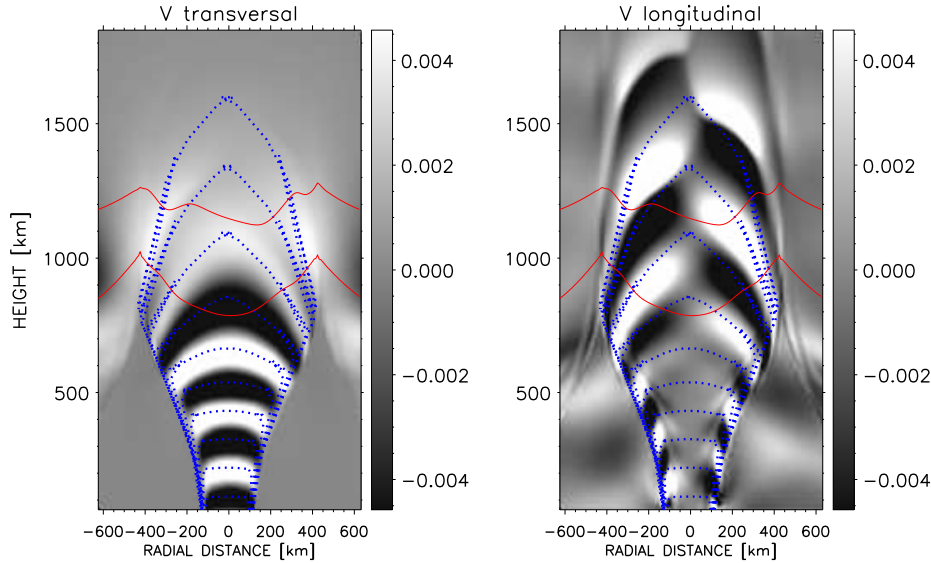


**Figure 4.** WKB solution for the simulations with a horizontal driver at 50 seconds. The format of the figure is the same as Figure 2. Blue contours are the positions of constant phase of the WKB slow mode solution at the different equidistant time moments.

can be appreciated from the time evolution of the simulation shown in Figure 3, where it is clear that significant perturbation in the longitudinal velocity in the upper layers inside the flux tube appears only after the slow mode reaches the transformation layer. Some of the energy of the slow magnetic mode also goes into the fast magnetic mode at the  $v_A > c_S$  region. As shown by the sequence of snapshots, this fast mode is refracted back to the photosphere. However, its energy is small compared to that of the slow acoustic mode in the  $v_A > c_S$  layers. The ratio of the transverse and longitudinal velocities at these heights is close to 0.1. This situation should be contrasted with the simulations of waves in sunspots (Khomenko and Collados, 2006), where a significant part of the energy of the driver was returned back to the photosphere by the fast magneto-acoustic mode. The slow acoustic mode in the  $v_A > c_S$  region is longitudinal and can be observed at heights above 1000 km in the longitudinal velocity snapshot. It propagates along the magnetic field lines straight up to the chromosphere and carries most of the energy of the driver to the upper heights. Motions on opposite sides of the flux tube are in anti-phase, as a natural consequence of the horizontal motions of the tube at the photospheric boundary.

The finding that the slow magnetic mode is effectively transformed into the slow acoustic mode is different from the conclusions of, *e.g.*, Bogdan *et al.* (2003) who obtain from their simulation that a significant part of the slow-mode energy goes into the fast mode, thus preserving the magnetic nature of the wave at all heights. In order to better understand our simulations, we present in Figure 4 the WKB solution for the slow mode. The WKB approach is linear and assumes that the wavelength of the perturbation is much smaller than the characteristic scale of the variations of the background atmospheric parameters, and thus can be applied in the case of the short-wavelength simulations with the 50-seconds driver. The equations describing the WKB approach in this particular case can be found in Khomenko

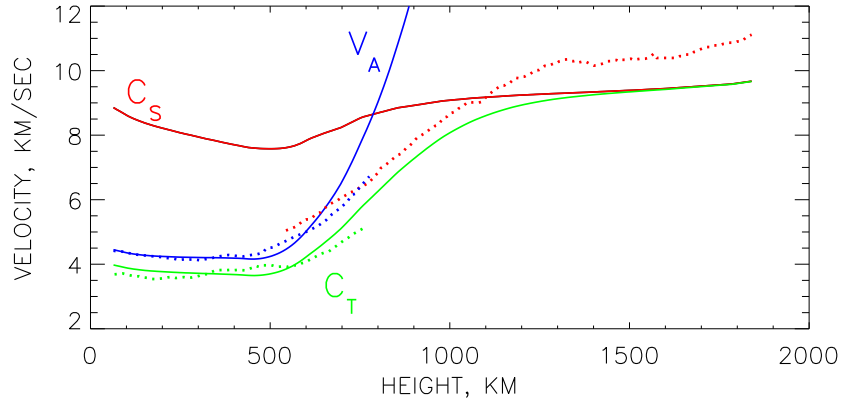


**Figure 5.** Height dependence of phase speeds of the slow mode (blue dotted line), surface mode (green dotted line) and acoustic mode (red dotted line) measured from the simulations compared to the characteristic propagation speeds calculated in the magnetostatic model (solid lines). The values of the Alfvén and sound speed ( $v_A$  and  $c_S$ ) are taken at the flux tube axis. The value of the tube speed ( $c_T$ ) is computed along the trajectory of the surface mode.

and Collados (2006). The blue contours in Figure 4 describe the position of the wave front at different time moments separated by equal intervals. The initial wavefront at the base of the atmosphere is assumed planar, *i.e.* the horizontal wave vector  $k_x$  is equal to zero. The WKB solution describes rather well the position of the wavefront at every time moment, *i.e.* the waves propagate at the slow-mode speed. As can be appreciated from the figure, as the wave propagates upwards, the horizontal gradients of its phase speed produce the deformation of the wave front, so that its central part propagates faster. It means that at greater heights the wave vector ( $\vec{k}$ ) is no longer directed along the vertical, but forms a significant angle with respect to the magnetic field vector  $\vec{B}_0$ . According to Cally (2006), if the angle between  $\vec{k}$  and  $\vec{B}_0$  is close to zero, the most effective transformation is from the slow to the fast mode. However, as this angle increases, the slow to slow mode transformation becomes more important. Since in our simulations the slow mode reaches the transformation layer with  $\vec{k}$  significantly inclined with respect to  $\vec{B}_0$ , it explains the effectiveness of the slow to slow mode transformation. This does not contradict the fact that the wave energy may propagate longitudinally, which is a result of the strong anisotropy of the medium.

The slow acoustic mode develops shocks with amplitudes of about  $5 \text{ km s}^{-1}$  that propagate straight up into the chromosphere. Due to the clear non-linear behavior of the acoustic mode at the greater heights, secondary harmonics are generated in addition to the frequency of the original perturbation of the driver. However, the maximum power at all heights is kept at the driving frequency.

Figure 5 gives the characteristic speeds of the waves in the simulation. Using the time series of the simulations, we have calculated the phase speed of the slow magnetic mode (at heights from 0 to about 800 km, where this mode exists), the slow acoustic mode (at heights from 500 km upward) and the surface mode. In the latter case, the phase speed along the curved trajectory of the surface mode was calculated. The retrieved phase speeds are displayed in Figure 5 as a function of

height. The stratifications of  $v_A$ ,  $c_S$  and tube speed ( $c_T^2 = c_S^2 v_A^2 / (c_S^2 + v_A^2)$ ) are also presented.

The comparison of the dotted and solid line curves in Figure 5 leads to coherent results. The slow magnetic mode propagates with the Alfvén speed ( $v_A$ ). The surface mode propagates with the tube phase speed ( $c_T$ ) up to 400 km. Despite the fact that the tube and the Alfvén velocities are rather similar in the lower photosphere, the phase speed of the surface wave is distinct from that of the slow magnetic wave. The former propagates with its own characteristic speed, as suggested from the analytical theory (see, *e.g.* Roberts, 1981). At heights about 700 km (where  $v_A \approx c_S$ ) the speeds of all modes become close to one another and the energy can be easily transferred between the different wave types. It can be seen that the slow magnetic mode and the surface mode give their energy to the slow acoustic mode. As the slow acoustic mode propagates upwards, shock formation occurs and the propagation becomes supersonic. The phase speed of the shocks increases with height in agreement with the increase of their amplitudes.

The following items summarize the most important features of the simulations with the horizontal driver at 50 seconds:

- Slow to slow mode transformation at the  $v_A = c_S$  height.
- Left-right acoustic shock wave pattern in anti-phase.
- Surface mode excitation.
- The period of the waves is maintained at all heights.

The simulation with this 50 seconds driver follows the spirit of the calculations by Rosenthal *et al.* (2002), Bogdan *et al.* (2003) and Hasan *et al.* (2005), where small scale flux tubes were perturbed by horizontal high-frequency motions at the lower boundary. Similarly to these works, we also find that such motions generate acoustic shocks at chromospheric heights. The differences in the wave behavior between these works and ours are mainly due to the difference in the initial magnetostatic situation. Once more, this suggests that the background magnetostatic state should be taken into account while interpreting observations, since different wave types can be generated.

## 6. Horizontal Driving at 180 Seconds

Here, we show the results of the simulations using a 180-seconds driver, still above the cut-off frequency. For this reason, it is not surprising that we get a behavior similar to the previous case. The wave pattern that appears in the simulations is basically the same as in the case of the 50 seconds driver, but the wavelength of the perturbations is larger. The driver mainly excites in the lower layers a transverse slow magnetic mode inside the flux tube, together with a surface mode at the interface with the non-magnetic surroundings. As before, the surface mode is mainly longitudinal. Figure 6 shows some snapshots of the transverse and longitudinal velocities during one period of the wave after the simulations reached the stationary state. In contrast to the case of the short-wavelength 50 seconds driver simulation, we find the normalization of the velocity components to  $\sqrt{c_S \rho_0}$  or  $\sqrt{v_A \rho_0}$  to be not appropriate for the 180 and 300 seconds driver simulations since the group velocity of waves follows a more

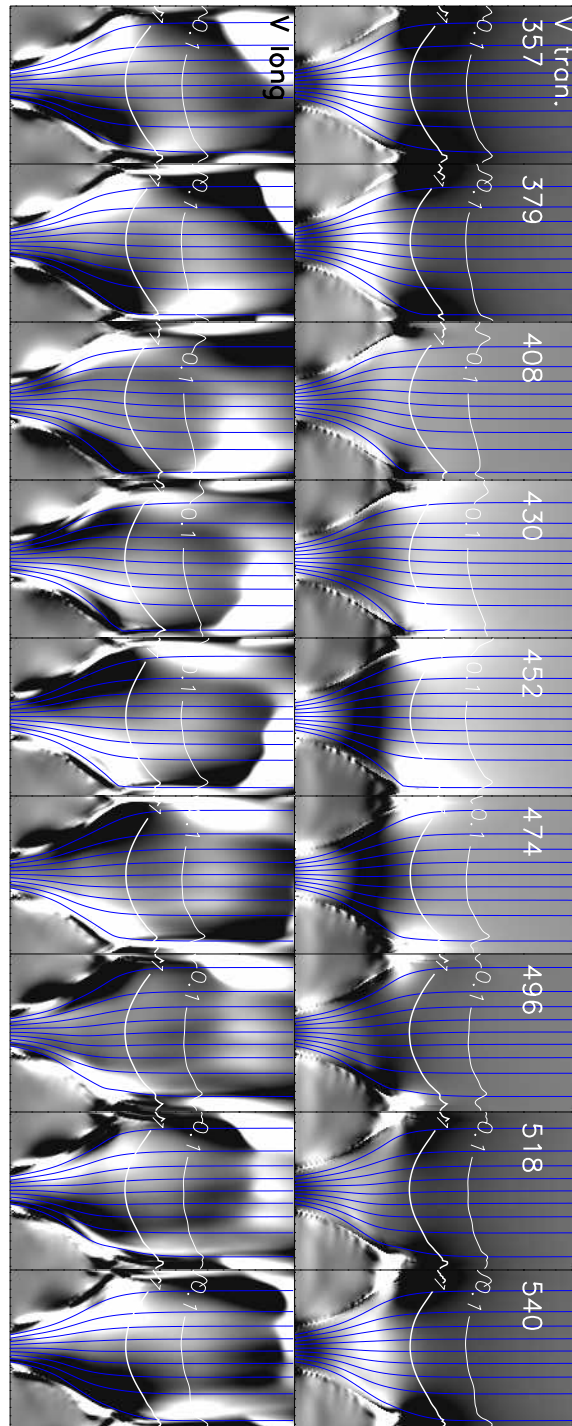


**Figure 6.** Time series of snapshots of the transverse (right) and longitudinal (left) velocities in the simulation with a horizontal driver at 180 seconds. Numbers give the elapsed time in seconds since the start of the simulation. After removing the average velocity increase with height produced by the density fall-off, all images have the same scale. Each snapshot includes 900 km in horizontal and 2000 km in vertical direction.

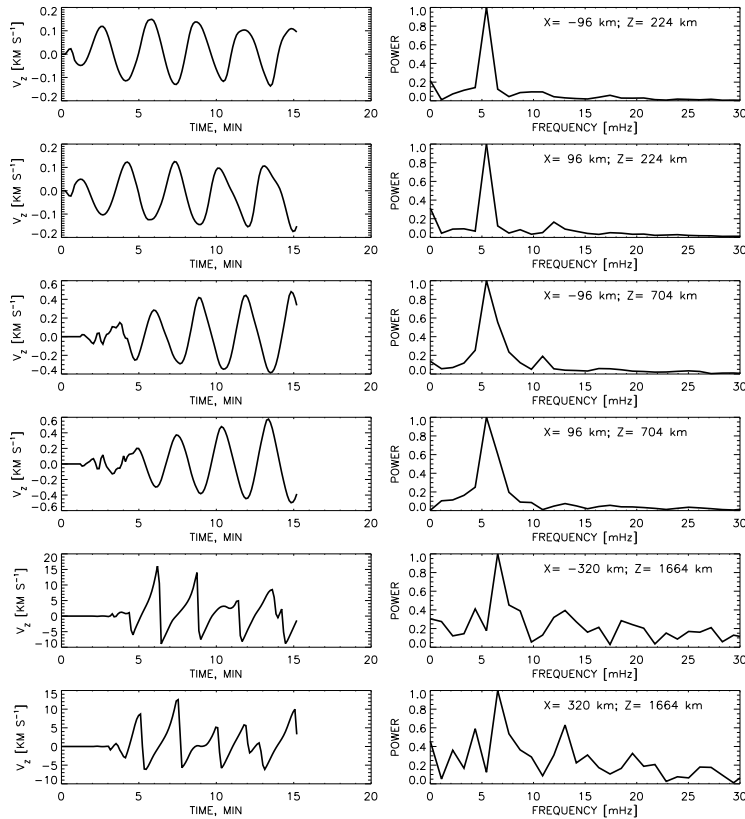


**Figure 7.** Examples of the temporal evolution of the longitudinal velocity (left) and their corresponding power spectra (right) at different heights and positions inside the flux tube for the simulation with horizontal driving at 180 seconds. The coordinates are indicated on the right panels.

complicated behaviour than either  $c_S$  or  $v_A$  due to the larger wavelength and non-linear effects. Instead we normalize both velocity components with an exponential function ( $\rho_0^{1/4}$ ) that allows a better visualization of the results.

Around the  $c_s = v_A$  layer, mode conversion takes place and most of the energy goes again to the slow acoustic mode. The antisymmetric pattern with respect to the flux tube axis is still present in longitudinal velocity above this layer, although the antisymmetry is not as perfect as in the 50-seconds driver case. Shocks clearly develop during the evolution. Very clear examples are apparent at time 379 in the left part of the flux tube, and at time 452 in the right part. These non-linear effects are more pronounced in the higher layers. The shock formation occurs above a height of about 1000 km. The temporal evolution of the transverse velocity shows the refraction of the fast magnetic mode at the higher layers where  $v_A > c_S$ . The horizontal motions of the flux tube field lines in the photosphere and chromosphere due to this mode can also be seen during the time evolution.

In Figure 7, the temporal evolution of the longitudinal velocity at different points in the flux tube, corresponding to different heights and horizontal distances from the axis, is shown. The first two upper panels on the left correspond to two points

located near the boundary of the flux tube, one on the right and the other on the left of the axis, 200 km above the driver. The almost sinusoidal oscillation pattern is clear, since non-linearities have not had time to develop. When comparing the position in the horizontal axis of maxima and minima for the velocity time series from both points, it is apparent that both points oscillate in anti-phase. The two middle panels on the left correspond to two points located at the same distance from the axis than the previous ones, but at a larger height (704 km). This is the height where  $v_A \approx c_S$  and the wave transformation starts. The amplitude of the oscillation has increased by almost a factor of four. It can be seen how the wave takes some time to reach this layer. The perturbation reaches this layer about four minutes after the driver starts. Up to there, non-linearities are still negligible, and the sinusoidal aspect of the wave is still kept, as well as this antisymmetry of the velocity pattern. At higher layers (1664 km in the plots) velocity discontinuities appear, indicating the development of shocks, with amplitudes of several  $\text{km s}^{-1}$  (two bottom panels of Figure 7). The corresponding power spectra of this velocity temporal series are plotted in the right-hand part, and they all demonstrate that the frequency of the driver (5.56 Hz) remains unaltered at all heights. The presence of several harmonics in higher layers is indicative of the non-linearities giving rise to the saw-tooth velocity profiles, rather than sinusoidal. Note that the shocks are in antiphase at the both sides of the tube.

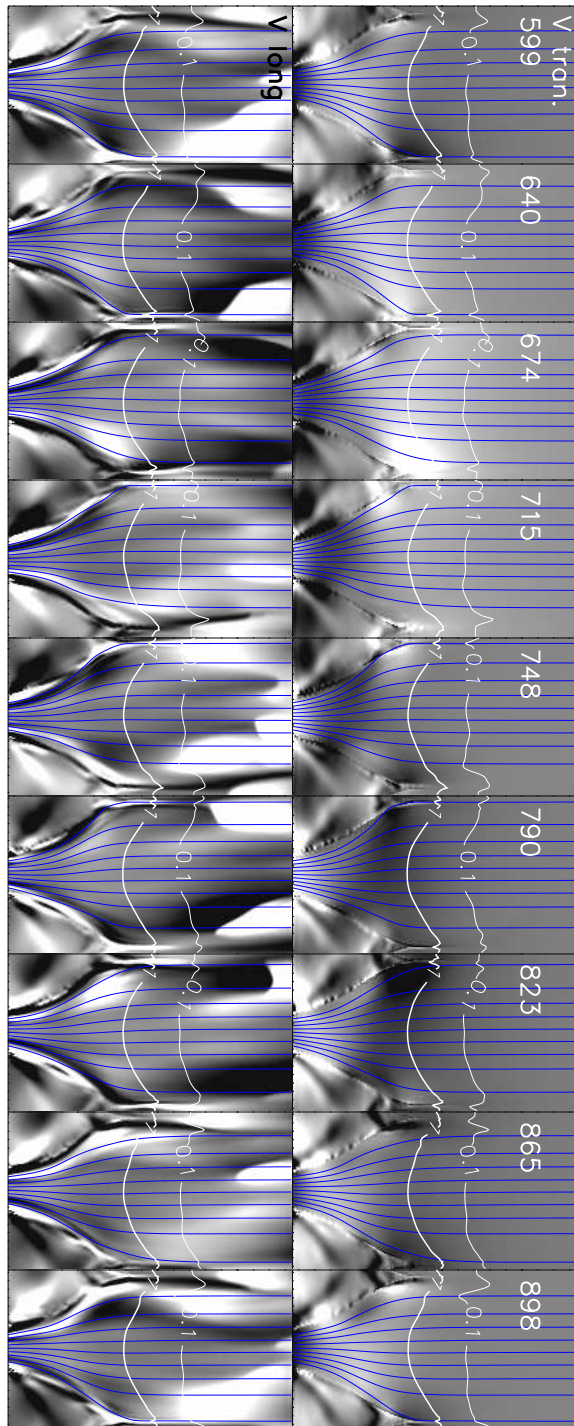
Probably, the most important difference with respect to the previous case with a driver of 50 seconds, lies in the fact that the slow-to-slow mode conversion is not as efficient now (see Cally, 2006), and a larger part of the energy of the slow mode excited by the driver is transferred to the fast (transverse, and hence, mainly magnetic) mode. The atmosphere above the  $v_A = c_S$  oscillates uniformly to left and right with small phase differences. The horizontal motions are in phase in the whole atmosphere due to the large oscillation wavelength.

Summarizing, the most important features of the simulations with the horizontal driver at 180 seconds are:

- Partial slow to slow (acoustic) transformation at  $v_A = c_S$  height.
- Horizontal flux tube motion at 2000 km due to the fast (magnetic) wave.
- Left-right shock wave pattern in anti-phase.
- Surface mode excitation.
- Period of the wave maintained with height.

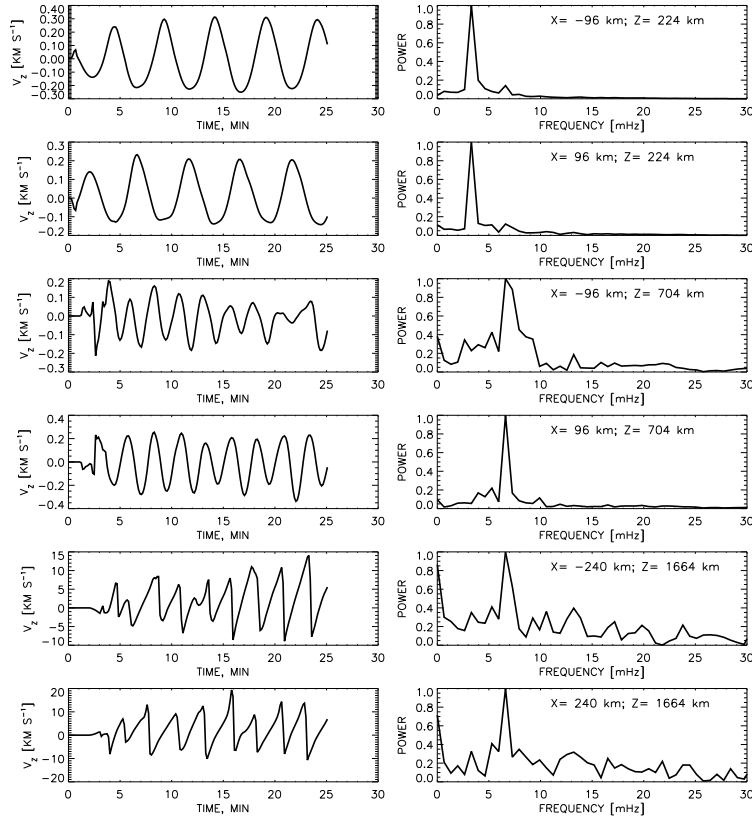
## 7. Horizontal Driving at 300 Seconds

Figure 8 shows the temporal evolution of the transverse and longitudinal velocities over one wave period, after the simulations reach the stationary state, and Figure 9 gives the temporal variation of the longitudinal velocity at selected points, together with their corresponding power spectra, for the simulations with a horizontal driver with a period of 300 seconds. The frequency of the driver is below the cut-off frequency. As in two previous cases, the driver excites the slow and surface modes. Note that, unlike the shorter-period simulations, there are significant motions excited outside the flux tube in the non-magnetic atmosphere as well. The nature of these motions is partly acoustic and partly convective since the lower layers of the photosphere are still unstable to convection.



**Figure 8.** Time series of snapshots of the transverse (right) and longitudinal (left) velocities in the simulation with a horizontal driver at 300 seconds. Numbers give the time elapsed in seconds since the start of the simulation. After removing the average velocity increase with height produced by the density fall-off, all images have the same scale. Each snapshot includes 900 km in horizontal and 2000 km in vertical direction.





**Figure 9.** Examples of the temporal evolution of the longitudinal velocity (left) and their corresponding power spectra (right) at different heights and positions inside the flux tube for the simulations with horizontal driving at 300 seconds. The coordinates are indicated on the right panels.

The slow-to-slow mode transformation is only partial, and part of the energy of the slow mode is transferred to the fast mode above the  $v_A = c_S$  layer, producing a horizontal shaking of the tube that propagates upwards with the Alfvén speed. The behavior of the fast mode seen in the transverse velocity above  $v_A = c_S$  height is similar to the three-minute period simulations, but the left-right symmetry pattern is lost.

Most of the energy in high layers is nonetheless still carried by the slow (acoustic) mode, giving rise to shock waves with amplitudes of  $10 - 15 \text{ km s}^{-1}$  above 1000 km height. The antisymmetric nature of these shocks has disappeared. Left and right parts of the tube are almost in phase now. However, the most conspicuous difference lies in the period of the wave. As it corresponds to an evanescent wave, the five-minute oscillation is rapidly damped, and the residuals coming from non-linear effects at 6 Hz, twice the driver frequency, already dominate at a height of 700 km. This double frequency is clear in the temporal series of the velocity, and in the corresponding power spectra, at this height (two middle panels in Figure 9). From 700 km upward, the velocity increases again, due to the density decrease, giving rise to shocks in the upper part of the simulation domain. The main frequency is maintained around 6

mHz, once the five-minute oscillation has been damped. Kalkofen *et al.* (1994) and Fleck and Schmitz (1991) showed that the change of the dominant period of acoustic oscillations with height, from five to three minutes, is due to the resonant excitation of waves at the atmospheric cut-off frequency (*i.e.* the cut-off frequency corresponding to the temperature minimum). However, this effect may not be dominant in our simulations since the acoustic mode only appears above 1000 km, *i.e.* well above the temperature minimum. At heights above 1000 km, the cut-off frequency is again around three mHz and the resonant excitation cannot produce oscillations at the higher frequency. We conclude that the generation of oscillations at the first harmonic of the driver in our simulations is mostly a non-linear phenomenon.

As in the previous sections, the most important properties of the wave propagation from the simulations with the horizontal driver at 300 seconds are:

- Partial slow to slow (acoustic) transformation at  $v_A = c_S$  height.
- Horizontal flux tube motion at 2000 km due to the fast (magnetic) wave.
- Left-right shock wave pattern in phase.
- Surface mode excitation.
- Period of the wave not maintained with height.

## 8. Vertical Driving at 300 Seconds

Finally, the results after exciting the flux tube with a 300-seconds vertical driver are presented. Figure 10 gives some snapshots of the velocity evolution during one period with the same format as in the previous figures. The time series shown in the figure is taken after the simulations reach the stationary state. Now, the fast (acoustic) wave is excited directly by the driver inside the flux tube in the deeper layers (see lower panels of Figure 10). The surface wave exists as well at the magnetic/field-free interface. There are some acoustic disturbances that can be observed in the field-free atmosphere surrounding the tube at the lower layers. After some time has elapsed since the start of the simulation, convective vortices appear in the non-magnetic atmosphere.

At the  $v_A = c_S$  layer, the fast to slow transformation occurs, keeping the acoustic nature of the wave. Almost no energy is transferred to the fast magnetic mode in high layers. It can be seen in the upper panels of Figure 10 that the transverse velocity inside the flux tube remains close to zero all of the time. The magnetic field lines are compressed and expanded as the wave passes through the atmosphere, but no horizontal motions are observed.

The perturbation is almost perfectly symmetric at all heights with respect to the tube axis, as demonstrated in the four upper panels of Figure 11, where the time series in symmetric positions inside the flux tubes are given. The most striking fact comes from the different behavior of the velocity at points near the tube axis or at the tube boundary in the upper heights. At deep layers, the propagation is mainly linear showing the five-minute sinusoidal pattern of the driver (see the upper panels in Figure 11). From there upwards, two shock waves develop at the beginning of the series, which are followed by a highly damped oscillation. The period of these shocks is three minutes. After the simulation reaches the stationary state, the dominant periods are different at the tube axis and off axis. For points near

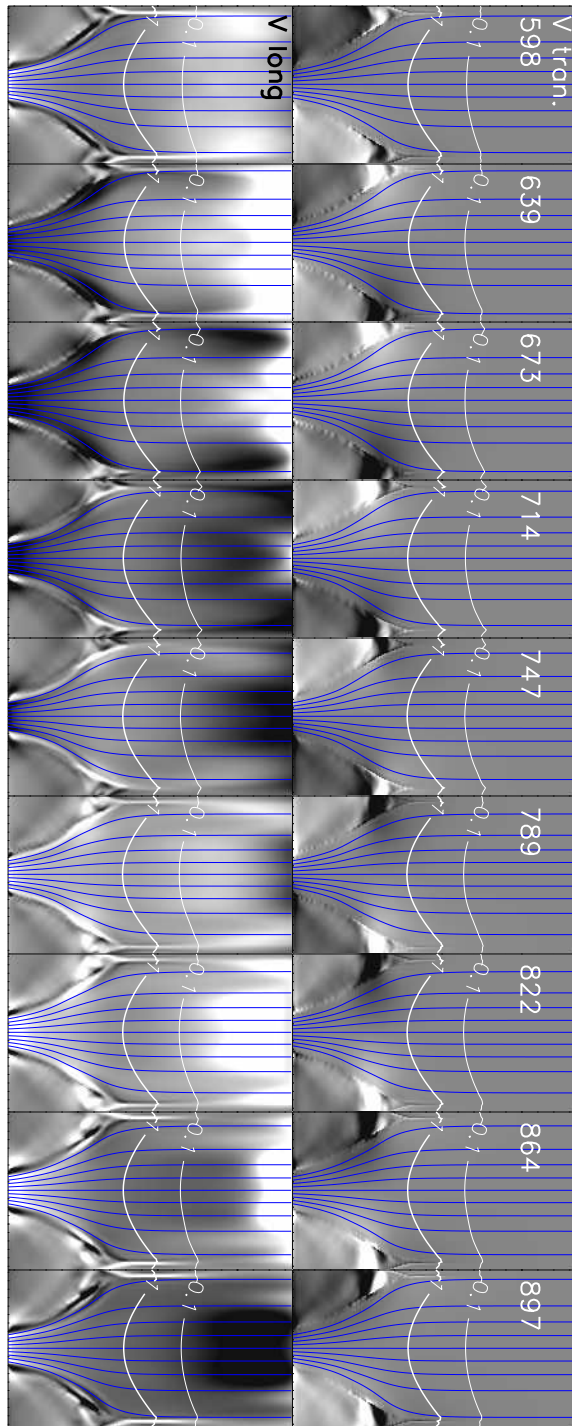


**Figure 10.** Time series of snapshots of the transverse (right) and longitudinal (left) velocities in the simulation with a vertical driver at 300 seconds. Numbers give time in seconds since the start of the simulation. After removing the average velocity increase with height produced by the density fall-off, all images have the same scale. Each snapshot includes 900 km in horizontal and 2000 km in vertical direction.

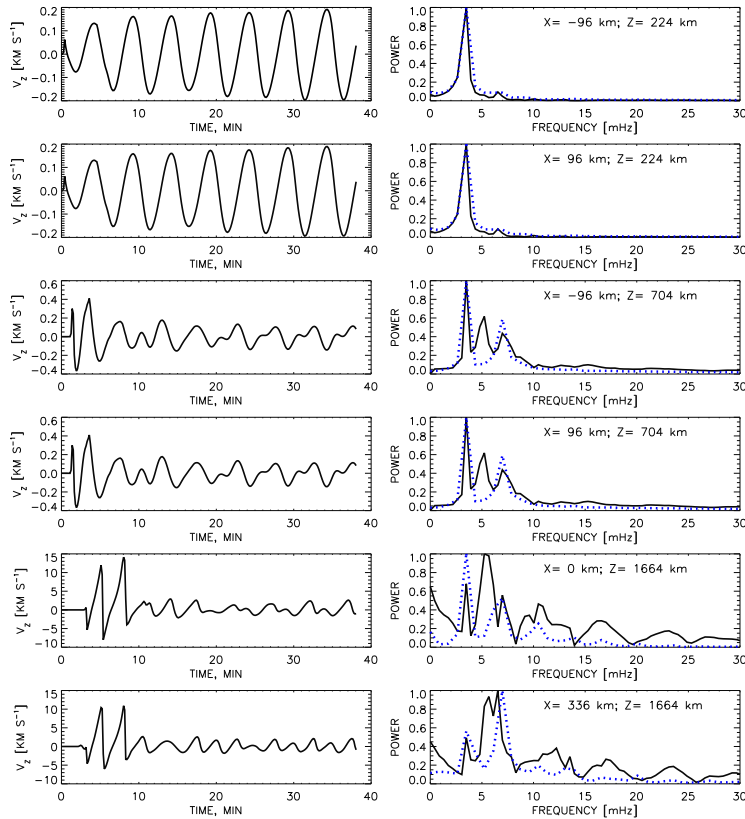


**Figure 11.** Examples of the time evolution of the longitudinal velocity (left) and their corresponding power spectra (right) at different heights and positions inside the flux tube in simulations with vertical driving at 300 seconds. The coordinates are indicated on the right panels. The blue dotted line at the right panels gives the power spectra only for the last half of the simulations after reaching the stationary state.

the axis, the five-minute oscillation does not suffer such a large amplitude damping and is the dominate period once the oscillation reaches a stationary state (see the power spectra corresponding to the second half of the simulation as a blue line in Figure 11). For off-axis points, there is a clear change with height of the dominating frequency. The contribution of the five-minute fundamental frequency is reduced as the wave propagates, increasing the relative importance of the first harmonic at 6 mHz (lower panel of Figure 11). Thus, in this simulation, 3 and 6 mHz oscillations coexist in different parts of the tube. In any case, the amplitudes are rather small when compared to those derived from horizontal drivers and only weak eventual shocks are observed with amplitudes of  $2 - 3 \text{ km s}^{-1}$ .

To summarize, the most important features of the simulations with a horizontal driver of 300 seconds are:

- Fast to slow transformation at  $v_A = c_S$  height.
- Weak eventual shocks
- Period on-axis: five minutes

- Period off-axis: three minutes

If the simulations with horizontal drivers can be understood in terms of mode transformation, and wave amplification/damping, this is not the case for this simulation with a 300-seconds vertical driver. Why does the main period of the wave above the  $v_A = c_S$  layer depend on the distance to the axis? Why do shocks develop at the beginning of the series and not later? More simulations are needed in different flux tubes, with varying initial conditions, to understand this complex behavior.

## 9. Discussion and Conclusions

We have performed simulations of waves in flux tubes with non-trivial magnetic field configuration. The model flux tube has horizontal and vertical variations of magnetic field strength and gas pressure and of the ratio between the characteristic wave speeds  $v_A$  and  $c_S$ . These properties have allowed us to study wave propagation and mode transformation inside the flux tube. Waves are excited by a photospheric driver with a period of three and five minutes, for the first time with a magnetic field configuration of this kind. Different wave patterns are observed depending on the period and on the type of the driver. The following items summarize our findings:

- Horizontal motions of the flux tube at the bottom photospheric boundary generate a slow magneto-acoustic mode inside the tube and a surface mode at the magnetic/field free interface.
- After the slow magneto-acoustic mode and the surface mode reach the height where  $v_A \approx c_S$ , their energy is effectively transformed into a slow acoustic mode in the high atmosphere where  $v_A > c_S$ . Only a small part of the driver energy is returned back to the photosphere by the fast magneto-acoustic mode.
- The slow acoustic mode propagates vertically along the magnetic field lines in the atmosphere where  $v_A > c_S$ , forms shock waves above 1000 km with amplitudes of  $5 - 15 \text{ km s}^{-1}$  and remains always within the same flux tube. Thus, it can deposit effectively most part of the energy of the driver into the chromosphere.
- If the frequency of the horizontal driver is above the acoustic cut-off, non-linear wave propagation in the tube occurs with the dominant period of the driver at all heights. Non-linear effects produce higher harmonics, but their amplitude is small.
- If the frequency of the horizontal driver is below the acoustic cut-off, the dominant period of the longitudinal velocity changes with height from five to three minutes due to non-linear generation of the higher harmonics.
- The five-minute vertical perturbation of the flux tube at the bottom photospheric boundary generates a fast acoustic mode that propagates upward through the transformation  $v_A = c_S$  layer, without changing its nature and forming only eventual shocks in the chromosphere.
- After reaching the stationary state in the simulations with a vertical driver at 300 seconds, both three and five minute oscillations co-exist inside the flux tube at chromospheric heights. The dominant period at the axis is five minutes and the off-axis dominant period is three minutes.

Our simulations suggest once again that the properties of waves observed in magnetic structures are the direct consequence of their magnetic configuration, temperature, magnetic field strength, and the height where the mode transformation occurs. When analyzing observations, it is important to know whether they correspond to the level below or above the layer  $v_A = c_S$ . If the motions that excite oscillations inside flux tubes are purely horizontal, no correlation may be observed between velocity variations measured in the photosphere and the chromosphere. This is because only an acoustic mode can be detected in observations (at least at disc center) since it produces significant vertical velocities, unlike the slow magnetic mode existing in the photosphere. The acoustic mode is only generated above 700 – 1000 km in our simulations with a horizontal driver. In contrast, if the driver that excites oscillations has a vertical component, the acoustic mode is generated already in the photosphere. In this case, the oscillations in vertical velocity are coherent at photospheric and chromospheric heights.

In general, both simulations with horizontal and vertical drivers with 300-second periodicity show the change of the dominant wave period with height. This property is different from observations of plage and network regions where the five minute periodicity is preserved also in the chromosphere (Lites, Rutten, and Kalkofen, 1993, Krijger *et al.*, 2001, De Pontieu, Erdelyi, and de Wijn, 2003, Centeno, Collados, and Trujillo Bueno, 2006, Bloomfield *et al.*, 2006, Vecchio *et al.*, 2007). While our study may help to identify the wave modes observed in small-scale magnetic structures, further work is needed in order to explain the behavior of the oscillatory spectra with height.

**Acknowledgements** The authors are grateful for the anonymous referee for his suggestions that helped to improve the manuscript. Financial support by the European Commission through the SOLAIRE Network (MTRN-CT-2006-035484) and by the Spanish Ministry of Education through projects AYA2007-66502 and AYA2007-63881 is gratefully acknowledged.

## References

- Bellot Rubio, L.R., Collados, M., Ruiz Cobo, B., Rodríguez Hidalgo, I.: 2000, Oscillations in the photosphere of a sunspot umbra from the inversion of infrared stokes profiles. *Astrophys. J.* **534**, 989–996.
- Berenger, J.P.: 1994, A perfectly matched layer for the absorption of electromagnetic waves. *J. Comp. Phys.* **114**, 185–200.
- Berger, T.E., Rouppe van der Voort, L., Löfdahl, M.: 2007, Contrast analysis of solar faculae and magnetic bright points. *Astrophys. J.* **661**, 1272–1288.
- Bloomfield, D.S., Lagg, A., Solanki, S.K.: 2007, Observations of running waves in a sunspot chromosphere. In: Heinzel, P., Dorotovic, I., Rutten, R.J. (eds.) *The Physics of Chromospheric Plasmas*, Astron. Soc. Pac. Conference Series, San Francisco, **368**, 239.
- Bloomfield, D.S., McAteer, R.T.J., Mathioudakis, M., Keenan, F.P.: 2006, The influence of magnetic field on oscillations in the solar chromosphere. *Astrophys. J.* **652**, 812–819.
- Bogdan, T.J., Carlsson, M., Hansteen, V., McMurry, A., Rosenthal, C.S., Johnson, M., Petty-Powell, S., Zita, E.J., Stein, R.F., McIntosh, S.W., Nordlund, A.: 2003, Waves in the magnetized solar atmosphere. ii. waves from localized sources in magnetic flux concentrations. *Astrophys. J.* **599**, 626–660.
- Bogdan, T.J., Judge, P.G.: 2006, Observational aspects of sunspot oscillations. In: *MHD wave and oscillations in the Solar Plasma*, Phil. Trans. Royal. Soc., **364**, Issue **1839**, 313–331.
- Braun, D.C., Lindsey, C.: 1999, Helioseismic images of an active region complex. *Astrophys. J.* **513**, L79–L82.

- Brynildsen, N., Maltby, P., Fredvik, T., Kjeldseth-Moe, O.: 2002, Oscillations above sunspots. *Solar Phys.* **207**, 259–290.
- Brynildsen, N., Maltby, P., Leifsen, T., Kjeldseth-Moe, O., Wilhelm, K.: 2000, Observations of sunspot transition region oscillations. *Solar Phys.* **191**, 129–159.
- Cally, P.: 2006, Dispersion relations, rays and ray splitting in magnetohelioseismology. *Royal Soc. London Trans. Series A* **364**, 333–349.
- Cally, P.: 2006, What to look for in the seismology of solar active regions. *Astronomische Nachrichten* **328**, 286.
- Carlsson, M., Stein, R.F.: 1997, Formation of Solar Calcium H and K Bright Grains. *Astrophys. J.* **481**, 500.
- Centeno, R., Collados, M., Trujillo Bueno, J.: 2006, Oscillations and wave propagation in different solar magnetic features. In: Casini, R., Lites, B.W. (eds.) *Solar Polarization 4*, Astron. Soc. Pac. Conference Series, San Francisco, **358**, 465.
- Centeno, R., Collados, M., Trujillo Bueno, J.: 2006, Spectropolarimetric investigation of the propagation of magnetoacoustic waves and shock formation in sunspot atmospheres. *Astrophys. J.* **640**, 1153–1162.
- Christopoulou, E.B., Georgakilas, A.A., Koutchmy, S.: 2000, Oscillations and running waves observed in sunspots. *Astron. Astrophys.* **354**, 305–314.
- Christopoulou, E.B., Georgakilas, A.A., Koutchmy, S.: 2001, Oscillations and running waves observed in sunspots. iii. multilayer study. *Astron. Astrophys.* **375**, 617–628.
- Collados, M., Trujillo Bueno, J., Bellot Rubio, L.R., Socas-Navarro, H.: 2001, In: Ballester, J.L., Roberts, B. (eds.) *INTAS workshop on MHD waves in astrophysical plasmas*. Universitat de les Illes Balears, 151–154.
- De Moortel, I., Ireland, J., Hood, A.W., Walsh, R.W.: 2002, The detection of 3 & 5 min period oscillations in coronal loops. *Astron. Astrophys.* **387**, L13–L16.
- De Pontieu, B., Erdelyi, R., de Wijn, A.G.: 2003, Intensity oscillations in the upper transition region above active region plage. *Astrophys. J.* **595**, L63–L66.
- De Pontieu, B., Erdelyi, R.J., Stewart, P.: 2004, Solar chromospheric spicules from the leakage of photospheric oscillations and flows. *Nature* **430**, 536–539.
- Fleck, B., Schmitz, F.: 1991, The 3-min oscillations of the solar chromosphere - a basic physical effect? *Astron. Astrophys.* **250**, 235–244.
- Fleck, B., Schmitz, F.: 1993, On the interactions of hydrodynamic shock waves in stellar atmospheres. *Astron. Astrophys.* **273**, 671.
- Gurman, J.B., Leibacher, J.W.: 1984, Linear models of acoustic waves in sunspot umbrae. *Astrophys. J.* **283**, 859–869.
- Hasan, S.S., Kalkofen, W., van Ballegooijen, A.A., Ulmschneider, P.: 2003, Kink and longitudinal oscillations in the magnetic network of the sun: Nonlinear effects and mode transformation. *Astrophys. J.* **585**, 1138–1146.
- Hasan, S.S., van Ballegooijen, A.A., Kalkofen, W., Steiner, O.: 2005, Dynamics of solar magnetic network: two-dimensional mhd simulations. *Astrophys. J.* **631**, 1270–1280.
- Hasan, S.S., Ulmschneider, P.: 2004, Dynamic and heating of the magnetic network on the sun. efficiency of mode transformation. *Astron. Astrophys.* **422**, 1085–1091.
- Judge, P.G., Tarbell, T.D., Wilhelm, K.: 2001, A study of chromospheric oscillations using the soho and trace spacecraft. *Astrophys. J.* **554**, 424–444.
- Kalkofen, W., Rossi, P., Bodo, G., Massaglia, S.: 1994, Propagation of acoustic waves in a stratified atmosphere. *Astron. Astrophys.* **284**, 976–984.
- Khomenko, E., Collados, M.: 2006, Numerical modeling of magnetohydrodynamic wave propagation and refraction in sunspots. *Astrophys. J.* **653**, 739–755.
- Khomenko, E.V., Collados, M., Bellot Rubio, L.R.: 2003, Magnetoacoustic waves in sunspots. *Astrophys. J.* **588**, 606–619.
- Korn, G.A., Korn, T.M.: 2000, *Mathematical Handbook for Scientists and Engineers*. Dover.
- Krijger, J.M., Rutten, R.J., Lites, B.W., Straus, T., Shine, R.A., Tarbell, T.D.: 2001, Dynamics of the solar chromosphere. iii. ultraviolet brightness oscillations from trace. *Astron. Astrophys.* **379**, 1052–1082.
- Lites, B.W.: 1984, Photoelectric observations of chromospheric sunspot oscillations. II - propagation characteristics. *Astrophys. J.* **277**, 874–888.
- Lites, B.W.: 1986, Photoelectric observations of chromospheric umbral oscillations. iv. the caii h line and hei 1830. *Astrophys. J.* **301**, 1005–1017.
- Lites, B.W.: 1988, Photoelectric observations of chromospheric umbral oscillations. v - penumbral oscillations. *Astrophys. J.* **334**, 1054–1065.

- Lites, B.W., Rutten, R.J., Kalkofen, W.: 1993, Dynamics of the solar chromosphere. I - long-period network oscillations. *Astrophys. J.* **414**, 345–356.
- Lites, B.W., Thomas, J.H., Bogdan, T.J., Cally, P.S.: 1998, Velocity and magnetic field fluctuations in the photosphere of a sunspot. *Astrophys. J.* **497**, 464–482.
- Maltby, P., Brynildsen, N., Fredvik, T., Kjeldseth-Moe, O., Wilhelm, K.: 1999, On the sunspot transition region. *Solar Phys.* **190**, 437–458.
- Maltby, P., Brynildsen, N., Kjeldseth-Moe, O., Wilhelm, K.: 2001, Plumes and oscillations in the sunspot transition region. *Astron. Astrophys.* **373**, L1–L4.
- Marsh, M.S., Walsh, R.W.: 2005, Observed wave propagation along the sunspot magnetic field through the chromosphere, transition region and corona. In: *Chromospheric and Coronal Magnetic fields*, ESA SP, Noordwijk. **596**, 75.1.
- Marsh, M.S., Walsh, R.W.: 2006, p-mode propagation through the transition region into the solar corona. i. observations. *Astrophys. J.* **643**, 540–548.
- Pneuman, G.W., Solanki, S.K., Stenflo, J.O.: 1986, Structure and merging of solar magnetic fluxtubes. *Astron. Astrophys.* **154**, 231–242.
- Roberts, B.: 1981, Wave propagation in a magnetically structured atmosphere. i - surface waves at a magnetic interface. *Solar Phys.* **69**, 27–38.
- Roberts, B.: 1983, Wave propagation in intense flux tubes. *Solar Phys.* **87**, 77.
- Rosenthal, C.S., Bogdan, T.J., Carlsson, M., Dorch, S.B.F., Hansteen, V., McIntosh, S.W., McMurtry, A., Nordlund, A., Stein, R.F.: 2002, Waves in the magnetized solar atmosphere. i. basic processes and internetwork oscillations. *Astrophys. J.* **564**, 508–524.
- Rüedi, I., Solanki, S.K., Stenflo, J., Tarbell, T., Scherrer, P.H.: 1998, Oscillations of sunspot magnetic fields. *Astron. Astrophys.* **335**, L97–L100.
- Socas-Navarro, H., Trujillo Bueno, J., Ruiz Cobo, B.: 2000, Anomalous circular polarization profiles in sunspot chromospheres. *Astrophys. J.* **544**, 1141–1154.
- Thomas, J.H., Stanchfield, D.C.H.: 2000, Fine-scale magnetic effects on p-modes and higher frequency acoustic waves in a solar active region. *Astrophys. J.* **537**, 1086–1093.
- Tziotziou, K., Tsiropoula, G., Mein, N., Mein, P.: 2006, Observational characteristics and association of umbral oscillations and running penumbral waves. *Astron. Astrophys.* **456**, 689–695.
- Tziotziou, K., Tsiropoula, G., Mein, N., Mein, P.: 2007, Dual-line spectral and phase analysis of sunspot oscillations. *Astron. Astrophys.* **463**, 1153–1163.
- Roupe van der Voort, L.H.M.R., Rutten, R.J., Sütterlin, P., Sloover, P.J., Krijger, J.M.: 2003, La palma observations of umbral flashes. *Astron. Astrophys.* **403**, 277–285.
- Vecchio, A., Cauzzi, G., Reardon, K.P., Janssen, K., Rimmele, T.: 2007, Solar atmospheric oscillations and the chromospheric magnetic topology. *Astron. Astrophys.* **461**, L1–L4.
- Vernazza, J.E., Avrett, E.H., Loeser, R.: 1981, Structure of the solar chromosphere. III - models of the euv brightness components of the quiet sun. *Astrophys. J.* **45**, 635–725.
- Zhugzhda, Y.D.: 2007, *Astron. Letters* **in press**.
- Zhugzhda, Y.D., Locans, V.: 1981, Resonance oscillations in sunspots. *Sov. Astron. Lett.* **7**, 25.